Structure of a Novel Enzyme That Catalyzes Acyl Transfer to Alcohols in Aqueous Conditions‡

Irimpan Mathews,§ Michael Soltis,§ Mae Saldajeno,|| Grant Ganshaw,|| Rafael Sala,|| Walter Weyler,|| Marguerite A. Cervin,|| Gregg Whited,|| and Richard Bott*,||

Stanford Synchrotron Research Laboratory, 2575 Sand Hill Road, Menlo Park, California 94025, and Genencor, a Danisco Division, 925 Page Mill Road, Palo Alto, California 94304

Received February 5, 2007; Revised Manuscript Received May 22, 2007

ABSTRACT: The unusual architecture of the enzyme (MsAcT) isolated from *Mycobacterium smegmatis* forms the mechanistic basis for favoring alcoholysis over hydrolysis in water. Unlike hydrolases that perform alcoholysis only under anhydrous conditions, MsAcT demonstrates alcoholysis in substantially aqueous media and, in the presence of hydrogen peroxide, has a perhydrolysis:hydrolysis ratio 50-fold greater than that of the best lipase tested. The crystal structures of the apoenzyme and an inhibitor-bound form have been determined to 1.5 Å resolution. MsAcT is an octamer in the asymmetric unit and forms a tightly associated aggregate in solution. Relative to other structurally similar monomers, MsAcT contains several insertions that contribute to the oligomerization and greatly restrict the shape of the active site, thereby limiting its accessibility. These properties create an environment by which MsAcT can catalyze transesterification reactions in an aqueous medium and suggests how a serine hydrolase can be engineered to be an efficient acyltransferase.

The ability to catalyze acyl transfer reactions to alcohols and esters in water is an unrealized goal of biocatalysis. Such reactions would eliminate the need for protection and deprotection steps in synthesis and therefore reduce the environmental impact and cost of such chemistry. The opportunity to exploit the selectivity and catalytic efficiency in an economical media could remove cost bottlenecks in the synthesis of many bioproducts, in particular, commodity chemicals. Previously, the best candidates have been found in lipases, which belong to the α/β hydrolase family of enzymes. Lipases are now widely used for catalytic and stereospecific transesterification reactions, in both academic and industrial laboratories. These reactions, described by Sym (*1*) and Zaks and Klibanov (*2*), are alcoholysis reactions run in anhydrous solvents and have found application in chiral synthesis, regio-specific protection, and enantiomeric resolution. In order to promote a desired alcoholysis, these reactions are conducted in anhydrous solvents to prevent the hydrolysis of the target ester. A large body of literature has accumulated to guide the practitioner in the selection of enzyme, choice of solvent, reaction condition, substrate specificity, chiral selectivity, immobilization techniques, and reaction kinetics (*3*). Such reactions, however, possess limitations due to the requirement of anhydrous solvents and can become expensive. In this paper, we show that a novel enzyme from *Mycobacterium smegmatis* catalyzes alcoholysis in substantially aqueous media. We have determined the crystal structures of the apoenzyme and an inhibitor-bound form to 1.5 Å resolution and postulate that the unusual architecture of MsAcT[1] forms the mechanistic basis for favoring alcoholysis over hydrolysis in water.

EXPERIMENTAL PROCEDURES

Cloning of the Enzyme with Acyltransferase Activity from M. smegmatis. An enzyme with acyltransferase activity was purified from *Mycobacterium parafortuitum* ATCC 19686 (*4*). Two peptide sequences were obtained from the purified protein. The sequence of one peptide, KVPFFDAGSVISTDGVDGI, was determined by Edman degradation from cyanogen bromide cleavage of the purified enzyme. The sequence of the second peptide, GTRRILSFGDSLTWGWIPV, was determined using N-terminal sequencing. A BLAST search against the TIGR unfinished genome database identified a sequence of potential interest in *M. smegmatis*. This gene was amplified from *M. smegmatis* by PCR using the primers MsRBSF, 5′-CTAACAGGAGGAATTAACCATGGCCAAGCGAATTCTGTGTTTCGGTGATTCCCTGACCT-3′, and MspetBamR, 5′-GCGCGCGGATCCGCGCGCTTACAGCAGGCTCCGCACCTGTTCCGCGAGGGCCACCCCGA-3′, which create an *Nco*I site at the ATG start codon and add a *Bam*HI site after the stop codon.

The amplification of the gene was done by PCR using *Taq* DNA polymerase (Roche) as per the manufacturer's

‡ Coordinates for the native and inhibited enzymes are deposited in the Protein Data Bank as entries 2q0q and 2q0s, respectively.

* To whom correspondence should be addressed. E-mail: Rick.Bott@Danisco.com. Phone: 650-846-5832. Fax: 650-845-6508.

§ Stanford Synchrotron Research Laboratory.

|| Genencor.

[1] Abbreviations: MsAcT, enzyme from *Mycobacterium smegmatis* with acyltransferase activity; OPD, *o*-phenylenediamine; NPG, neopentyl glycol; PCR, polymerase chain reaction; MAD, multiwavelength anomalous data; DNA, deoxyribonucleic acid; GC/FID, gas chromatography/flame ionization detector; GC/MS, gas chromatography/mass spectrometry; IPTG, isopropyl β-D-thiogalactopyranoside; DMSO, dimethyl sulfoxide; LA, Luria agar; LB, Luria broth.

10.1021/bi7002444 CCC: $37.00
Published on Web 07/18/2007

instructions, with approximately 500 ng of chromosomal DNA from *M. smegmatis* as the template DNA and the addition of 1% DMSO to the PCR reaction mix. Ten picomoles of each of the primers MsRBSF and MspetBamR was added to the mix. The amplification cycle was 30 cycles of 95 °C for 1 min, 55 °C for 1 min, and 72 °C for 1 min.

The fragments obtained from the PCR reaction were separated on a 1.2% agarose gel, and a single band of the expected size of 651 bp was identified. This band was cloned directly into the pCR2.1 TOPO cloning vector (Invitrogen) and transformed into *Escherichia coli* Top 10 cells (Invitrogen) with selection on Luria agar (LA) containing 100 μg/mL carbenicillin and X-gal (20 μg/mL; Sigma-Aldrich) for blue/white selection and incubated overnight at 37 °C. Plasmid DNA was purified from a culture of one of the transformants using the Quikspin kit (Qiagen). The presence of the correct fragment was determined by restriction enzyme digest with *Eco*RI to release the fragment and sequencing using primers supplied by the pCR2.1 manufacturer (Invitrogen). The plasmid was designated pMSATNcoI. The plasmid pMSATNcoI was digested with *Nco*I/*Bam*HI (Roche), and the fragment was gel purified using the Qiagen gel purification kit. The fragment was ligated into the expression plasmid, pET16b (Novagen), also digested with *Nco*I/*Bam*HI T4 DNA ligase overnight at 16 °C. The ligation reaction was transformed into chemically competent *E. coli* Top 10 cells (Invitrogen), and transformants were selected on LA containing carbenicillin after overnight growth at 37 °C. Plasmid DNA was prepared from cultures of a transformant using the Quikspin kit (Qiagen), and the presence of the correct fragment was determined by restriction enzyme digest with *Nco*I/*Bam*HI. The correct plasmid was designated pMSATNcoI-1. This plasmid was transformed into the *E. coli* strain BL21(λDE3) pLysS (Novagen), with selection on LA containing carbenicillin (100 μg/mL). Cells were grown overnight at 37 °C; one transformant was selected and designated MSAcTNcoI-1.

Expression of MsAcT. In the following experiments, all cultures of MSAcTNcoI-1 were grown in solid or liquid media containing carbenicillin at a concentration of 100 μg/mL unless otherwise stated. Production of MsAcT for enzymatic analysis was done by inoculating 5 mL of Luria broth (LB) with carbenicillin with a single colony of MSATNcoI-1 and grown overnight at 37 °C with shaking at 200 rpm. This culture was used to inoculate 100 mL of LB containing carbenicillin to an OD_{600} of 0.1. The cultures were grown at 30 °C with shaking at 200 rpm until they reached an OD_{600} of 0.4. The expression of the *act* gene was then induced by the addition of 100 μM IPTG and the incubation continued overnight. Cultures were harvested by centrifugation (10 min at 7000 rpm; Sorvall SS34 rotor), the supernatant was removed, and the pellets were washed in 50 mM potassium phosphate buffer, pH 6.8. The cells were centrifuged again, the supernatants were removed, and the wet weight of the cells was determined. The cells were resuspended in 100 mM potassium phosphate buffer, pH 8.2, in a volume that was 4 times the wet weight. The resuspended cells were frozen at −70 °C. The cells were thawed and lysed in a French pressure cell. The MsAcT was purified as described below in the Selenomethionine Labeling of MsAcT section.

Preparation of Homologues. The genes encoding *Sinorhizobium meliloti* RSM02162, RGAE, and *E. coli* thioesterase were synthesized by DNA 2.0 (Menlo Park, CA). The genes were subcloned into the pET16b T7 expression vector (Novagen), and expression of the proteins was done in BL21(λDE3) pLysS cells as described in the Expression of MsAcT section for the cloning and expression of MsAcT. The 7-ACA gene was amplified from *M. parafortuitum* chromosomal DNA using the primers ACA-F, 5′-GGTGAAGTCGGTCCTCTGCTTTG-3′, and ACA-R, 5′-GCGGATCCTCAAAGTCCGAGCATCATGCGAA-3′. The sequence was identical to that of the *Agrobacterium tumefaciens* (radiobacter) (protein accession number AAD02335). The primer set added *Nco*I and *Bam*HI sites at the 5′ and 3′ ends, respectively, and the gene was cloned into pET16b and the protein expressed as described in the Expression of MsAcT section for the cloning and expression of MsAcT.

Partial Purification of Homologues by Gel Filtration. After preparation of cell lysates from strains expressing the homologues, as described in the Expression of MsAcT section for MsAcT cultures, the homologues were partially purified by gel filtration. The cell lysates were run on a Superdex 200 sizing column in 20 mM phosphate, pH 8.0, at 0.5 mL/min. The column was calibrated prior to running the samples with molecular mass standards (thyroglobulin, MW 669 kDa; aldolase, MW 158 kDa; ovalbumin, MW 43 kDa; ribonuclease, MW 14 kDa) and purified MsAcT. In this method, MsAcT eluted in the same volume as the aldolase.

Selenomethionine Labeling of MsAcT. A 500 mL preculture of MsAcTNcoI-1 was grown in a baffled 2.8 L Fernbach flask in LB containing carbenicillin. After overnight incubation at 37 °C with shaking at 200 rpm, the cells were harvested by centrifugation and resuspended in M9 medium containing glucose (2 g/L), Na_2HPO_4 (6 g/L), KH_2PO_4 (3 g/L), NH_4Cl (1 g/L), NaCl (0.5 g/L), thiamin (5 mg/L), $MgSO_4$ (2 mM), $CaCl_2$ (100 μM), citric acid·H_2O (40 mg/L), $MnSO_4$·H_2O (30 mg/L), NaCl (10 mg/L), $FeSO_4$·$7H_2O$ (1 mg/L), $CoCl_2$·$6H_2O$ (1 mg/L), $ZnSO_4$·$7H_2O$ (1 mg/L), $CuSO_4$·$5H_2O$ (100 μg/L), H_3BO_3·$5H_2O$ (100 μg/L), and $NaMoO_4$·$2H_2O$ (100 μg/L) and supplemented with carbenicillin. The resuspended cells were used to inoculate six Fernbach flasks containing 500 mL each of M9 medium supplemented with carbenicillin. The cultures were incubated at 30 °C with shaking at 200 rpm until the OD_{600} reached about 0.7, at which time 100 mg/L lysine, threonine, and phenylalanine and 50 mg/L leucine, isoleucine, valine, and selenomethionine (EMD Biosciences) were added. After further incubation for 30 min, IPTG was added to a final concentration of 50 μM. The cultures were then incubated overnight (~15 h) at 30 °C with shaking at 200 rpm and harvested by centrifugation. The cell pellet was washed two times with 50 mM potassium phosphate buffer, pH 6.8. The yield was 28.5 g (wet weight) of cells to which was added 114 mL of 100 mM potassium phosphate buffer, pH 8.2, and 5 mg of DNase. This mixture was subjected to two freeze−thaw cycles (−70 °C and 4 °C).

The thawed cell suspension was lysed by disruption in a French pressure cell at 20000 psi. The unbroken cells and cell membrane material were sedimented by centrifugation at 100000*g* for 1 h. The supernatant crude extract (128 mL) was then placed in a 600 mL beaker and stirred for 10 min

in a 55 °C water bath to precipitate unstable proteins. After 10 min, the beaker was stirred in ice water for 1 min followed by centrifugation at 15000*g* for 15 min. The volume of the supernatant from this procedure was 118 mL. To this extract was added $(NH_4)_2SO_4$ to 20% saturation, and the resultant mixture was loaded onto a 10 cm × 11.6 cm fast-flow phenyl-Sepharose (Pharmacia) column equilibrated in 100 mM potassium phosphate buffer, pH 6.8, containing a 20% saturation (109 g/L) of $(NH_4)_2SO_4$. After the extract was loaded, the column was washed with 1700 mL of starting buffer and eluted with a two-step gradient. The first step was a linear 1900 mL gradient from start buffer to the same buffer without $(NH_4)_2SO_4$; the second step was a 500 mL elution with 100 mM potassium phosphate buffer, pH 6.8, containing 5% EtOH. The active fractions were pooled, giving a total volume of 241 mL, diluted 100% with water, and loaded onto a 1.6 mm × 16 mm Poros HQ strong anion-exchange column equilibrated in 100 mM Tris-HCl, pH 7.6. After the pooled fractions were loaded, the column was washed with 5 column volumes of starting buffer. The protein was eluted with a 15 column volume gradient from start buffer to start buffer containing 175 mM KCl. The active fractions were pooled and concentrated using a Centriprep 30 (Millipore) to 740 μL.

Transesterification. Reactions were conducted in single phase conditions of water dissolved in ethyl acetate or ethyl acetate dissolved in water. Each reaction contained 100 mM neopentyl glycol (NPG) in ethyl acetate with the indicated amount of dissolved water or 100 mM NPG dissolved in water containing 6% ethyl acetate in a final volume of 0.1 mL. The enzyme was added to a final concentration of 525 ng/mL in 2.5 μL of 1 μM potassium phosphate buffer and incubated at 21 °C. Samples were withdrawn at intervals for up to 30 min, and the product was separated and quantified by GC/MS on a 30M, BPX70 column (SGE Incorporated). Specific activity is reported as micromoles of NPG monoacetate produced per minute per milligram of MsAcT.

Inhibition of MsAcT with p-Nitrophenyl n-Hexylcarbamate. The inhibitor, 4′-nitrophenyl *n*-hexylcarbamate, was prepared as described by Hosie et al. (*5*). Purification was achieved by two recrystallizations in hexanes. ^1H and ^{13}C NMR spectra gave the expected signals.

MsAcT was added at a concentration of 12 mg/mL to 1 mL of 67 mM sodium phosphate buffer at pH 7 also containing 15% DMSO by volume. The mixture was incubated at 25 °C and stirred with a small magnetic stir bar. Inactivation was initiated by addition of a 10 μL aliquot of a 400 mM solution of inhibitor in DMSO. Six more 10 μL additions of the same inhibitor solution were made at 19, 51, 110, 166, 180, and 220 min, respectively. The reaction was terminated at 250 min by treatment of the sample with a spin column centrifugation through a column packed with 10.7 mL of Bio-Gel P-6. The column had been prepared by preequilibrating it with 10 mM HEPES buffer, pH 8, and centrifuging at 2000 rpm for 2 min in an IEC model HN-SII clinifuge swinging bucket rotor prior to loading the sample onto the column and centrifuging under the same conditions of time and speed to effect buffer exchange and removal of excess inhibitor and DMSO. Enzyme assay with *p*-nitrophenyl butyrate showed the enzyme to be >99% inhibited.

Determination of the Perhydrolysis/Hydrolysis Ratio. The rate of perhydrolysis was determined in reactions containing 50 mM potassium phosphate, pH 7.5, 10 mM tributyrin, 29 mM hydrogen peroxide, 20 mM potassium chloride, and 10 mM *o*-phenylenediamine (OPD) in a volume of 1.0 mL. Activity was measured by monitoring the absorbance increase at 458 nm of OPD, which was oxidized by perbutyric acid generated with the enzyme. The OPD solution was prepared immediately before use in assay buffer and the pH readjusted with potassium hydroxide. A quenching solution was prepared containing 10 mM OPD and 100 mM citric acid in 70% ethanol. The assay was conducted at 25 °C and was initiated by the addition of enzyme. Aliquots were taken at intervals over an hour and quenched with 2 volumes of quenching solution at appropriate times, typically 2, 5, 10, 15, 25, 40, and 60 min, after addition of the enzyme. The quenched assay samples were incubated for 30 min to allow any remaining perbutyric acid to oxidize the OPD, and then the absorbance was measured. The concentration of perbutyric acid was determined by comparison to a standard curve generated under the same conditions.

The rate of tributyrin hydrolysis was measured in reactions comprised of 50 mM potassium phosphate buffer, pH 7.5, 10 mM tributyrin, 29 mM hydrogen peroxide, and 20 mM potassium chloride and an amount of enzyme that would generate 20 μM butyric acid/min at 25 °C. Aliquots were taken at intervals over an hour and quenched with 4 volumes of methanol. The methanol-quenched samples were then analyzed by GC/FID (Zebron FFAP, 30 m long, 250 μm diameter, 250 nm film thickness). This assay was conducted under the same conditions as for perhydrolysis, i.e., in the presence of hydrogen peroxide, but with no trap for the perbutyric acid (OPD). Injection into the GC for analysis converts perbutyric acid to butyric acid; thus, the observed butyric acid signal represents enzymatically generated products, butyric acid and perbutyric acid. The actual amount of butyric acid generated in the assay was calculated by subtraction of the concentration of perbutyric acid (determined by OPD analysis) from the total butyric acid determined by GC/FID analysis.

The amount of enzyme used to determine the perhydrolysis/hydrolysis ratio reported in Figure 2 was that required to give a measurable and linear rate of tributyrin hydrolysis as described above. The enzyme source and concentration of each enzyme used were as follows: MsAcT (*4*), 4 μg/mL; AcT from *M. parafortuitum* (MpAcT) (*6*), 4 μg/mL; *Pseudomonas mendocina* cutinase (*7*), 2 μg/mL; *Candida cylindracea* cholesterol esterase (Roche Diagnostics), 2 μg/mL; *Rhizopus oryzae* lipase (Biocatalytics), 18 μg/mL; *Pseudomonas cepacia* lipase (Biocatalytics), 30 μg/mL; *Pseudomonas fluorescens* lipase (Biocatalytics), 20 μg/mL; *Candida antarctica* lipase B (Biocatalytics), 4 μg/mL; *C. antarctica* lipase A (Biocatalytics), 8 μg/mL; *Pseudomonas* sp. lipase (Biocatalytics), 17 μg/mL; porcine pancreatic lipase (Biocatalytics), 50 μg/mL; *Thermomyces lanuginosa* lipase (Biocatalytics), 3 μg/mL; *Mucor miehei* lipase (Biocatalytics), 3 μg/mL; and *Alcaligenes* sp. lipase (Biocatalytics), 14 μg/mL.

Crystal Preparation. Crystals were grown by the hanging drop vapor diffusion method. Native crystals were grown by mixing 4 μL of protein solution at 12.7 mg/mL concentration in 20mM HEPES buffer pH 8.0 with 6 μL of a

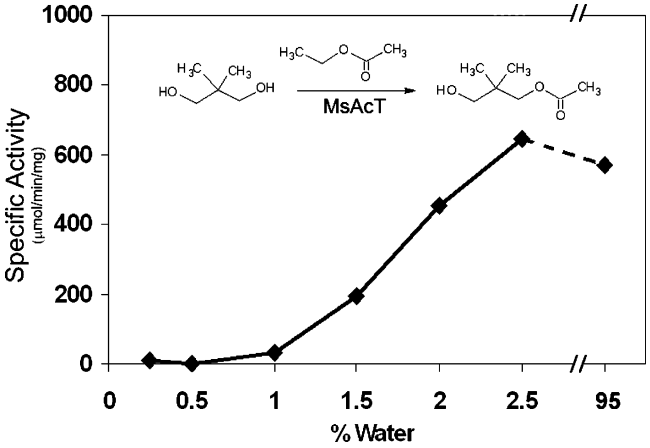

FIGURE 1: Catalytic activities of MsAcT: Transesterification of the acetate moiety from ethyl acetate to NPG in the presence of varying concentrations of water. Reactions were conducted under conditions yielding single phase mixtures of water dissolved in ethyl acetate or ethyl acetate dissolved in water; NPG was used at a concentration of 100 mM.

reservoir solution (2M ammonium sulfate, 2% polyethylene glycol 400, 0.1M Tris pH 8.1). Inhibited crystals were grown by mixing 2 μL of protein solution at 15 mg/mL in the same buffer with 4 μL of a reservoir solution (0.2M lithium sulfate, 30% polyethylene glycol 4000, and 0.1M Tris pH 8.5). Crystals appeared in 1 week and reached their maximum size within 3 weeks. Crystals of the selenomethionine derivative of MsAcT were obtained from hanging drops mixed with equal volumes of 22.7 mg/mL protein solution in 20 mM HEPES, pH 8.0, and a reservoir solution comprising 1.0 M ammonium dihydrogen phosphate and 100 mM sodium citrate, pH 5.6. The crystals were transferred to a reservoir solution and mixed in a 3:1 ratio with glycerol before cryocooling by immersion in a liquid nitrogen bath.

X-ray Data Collection. Multiwavelength anomalous diffraction (MAD) data were collected for the apoenzyme at the Advanced Light Source (ALS, Berkeley, CA) onbeamline 8.2.1 at wavelengths corresponding to the inflection (λ_1), low-energy remote (λ_2), and the peak (λ_3) of a selenium MAD experiment. Later, a data set (λ_0) was collected on beamline 8.2.2 to 1.5 Å resolution. The data sets were collected at 100 K using Quantum 210 CCD for the MAD data set and Quantum 315 CCD for the high-resolution data set. Data were integrated using Mosflm (*8*) and scaled with the SCALA program from the CCP4 suite (*9*). Data statistics are summarized in Table 2.

Diffraction data for the inhibitor-bound form were collected at the Stanford Synchrotron Radiation Laboratory (SSRL, Menlo Park, CA) on beamline 9-1. Crystals diffracted to better than 1.2 Å resolution. However, a complete data set was collected to only 1.5 Å resolution. The data set was collected at 100 K using Quantum 315 CCD and processed using the HKL2000 program suite (*10*). Data statistics are summarized in Table 2.

Structure Solution and Refinement. The initial structure was determined using the 2.5 Å selenium MAD data ($\lambda_{1,2,3}$) using the CCP4 suite and SOLVE/RESOLVE programs (*11*). Model building was performed using O (*12*). The traced model was then refined with the 1.5 Å data set (λ_0) using REFMAC (*9*). Refinement statistics are summarized in Table 2. The final model includes a protein octamer, 8 sulfate ions, 8 glycerol molecules, and 1608 water molecules in the asymmetric unit. No electron density was observed for the first methionine residue in any of the molecules. PROCHECK11 (*13*) indicates that 94% of the residues in all of the monomers are located in the core regions of the Ramachandran plot (*14*) with no residues in the disallowed or generously allowed regions.

The inhibitor structure was solved by molecular replacement with MOLREP (*13*) using the coordinates of the apoenzyme. Refinement statistics are summarized in Table 2. The final model includes a protein octamer, 8 inhibitor molecules, 1 sulfate ion, and 2134 water molecules in the unit cell. No electron density was observed for any of

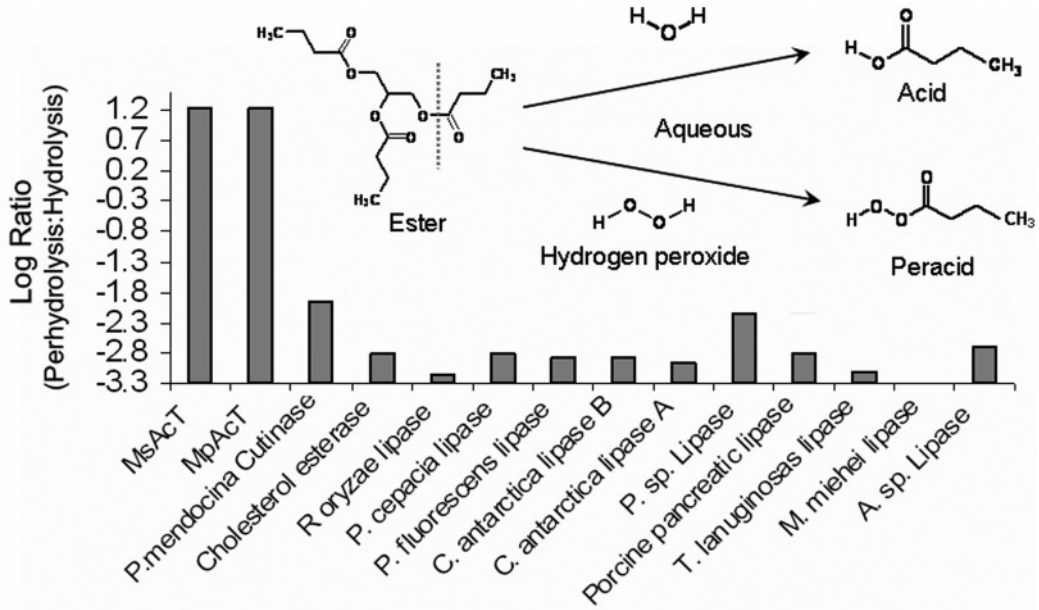

FIGURE 2: Selectivity of perhydrolysis to hydrolysis catalyzed by MsAcT and other lipases in the presence of 10 mM tributyrin and 30 mM hydrogen peroxide. MsAcT shows a high degree of selectivity for perhydrolysis over hydrolysis compared with other enzymes known to hydrolyze tributyrin.

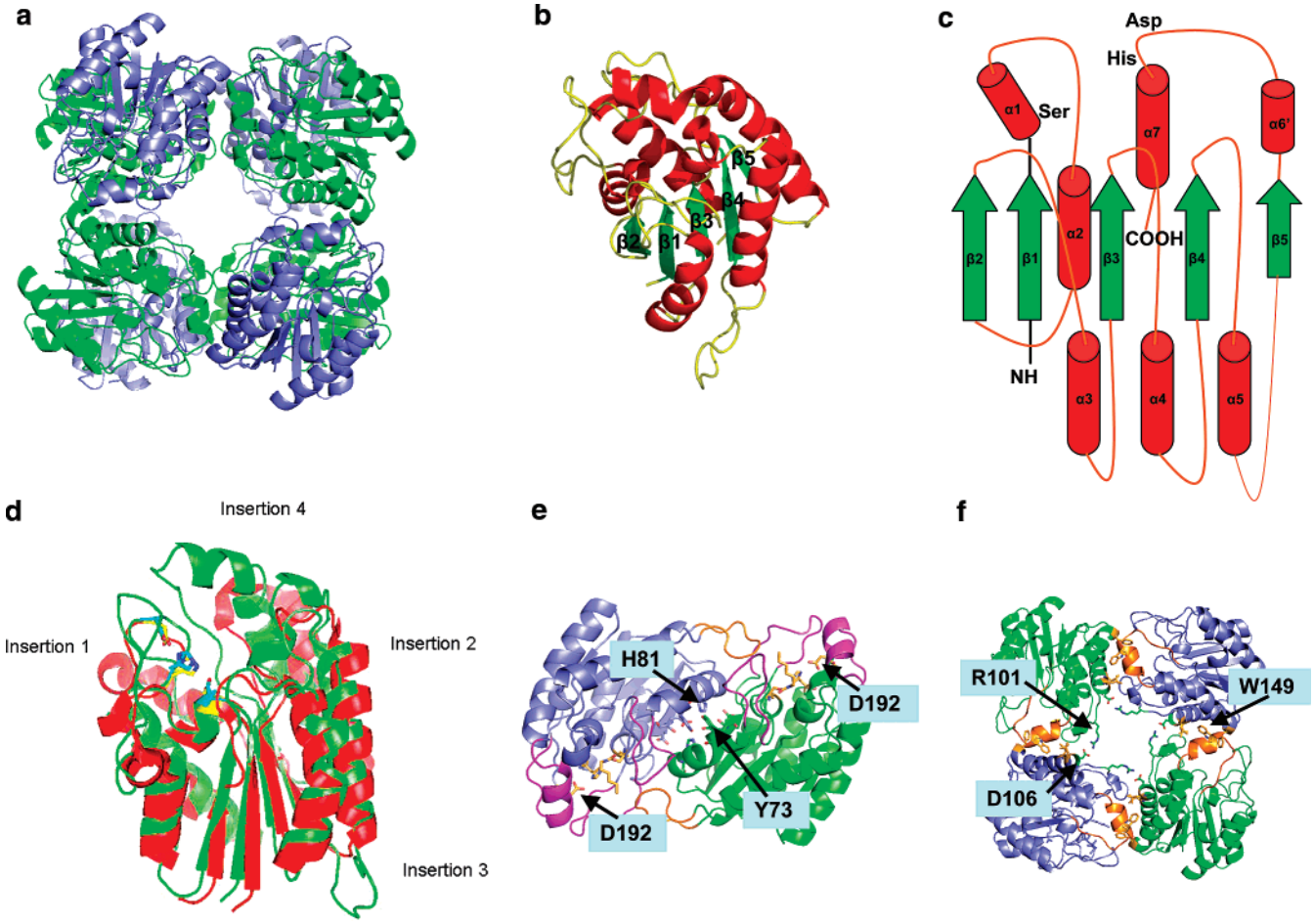

FIGURE 3: Structure of MsAcT. (a) Organization of the MsAcT octamer. The dimer pairs are colored green and blue. (b) Structure of the MsAcT monomer. The five-stranded β-sheet is labeled. (c) Schematic view of the SGNH hydrolase fold showing five parallel β-strands labeled $\beta1-\beta5$ and helices labeled $\alpha1-\alpha7$. The location of the catalytic triad residues is shown. (d) Comparison of the MsAcT monomer (colored green) with the thioesterase structure (colored red). (e) Interactions at the dimer interface. Insertion loop 3 (residues 122−130) from one dimer is shown in orange and insertion loops 1, 2, and 4 of the dimer mate are shown in magenta. Some of the key residues are labeled. (f) Interaction in the octamer. Insertion loop 4 that interacts with the dimer mate is highlighted in orange. Some of the residues discussed in the text are labeled.

Table 1: Characterization of Acyltransferase and Perhydrolysis Activity of MsAcT-Related Enzymes[a]

	acyltransferase activity[b]	perhydrolysis activity[b]	soluble aggregate[c]	sequence identity (%)[d]	structure
MsAcT	++++	++++	octamer	100	SGNH hydrolase
S. meliloti RSM02162	nd	++	apparent octamer	63.3	unknown
A. tumefaciens 7-ACA	+	+	tetramer (*14*, *15*)	42.5	unknown
E. coli thioesterase	−	−	monomer (*17*)	14	SGNH hydrolase
A. aculeatus rhamnogalacturonan acetylesterase	−	−	monomer (*18*)	13.8	SGNH hydrolase

[a] Either by sequence or structural homology. [b] Acyltransferase and perhydrolysis activities are presented as relative to the activity of MsAcT (++++) in the indicated assay. Assays were done as described in the Experimental Procedures. [c] Formation of multimers in solution was determined by gel filtration (MsAcT and RSM02162) or gathered from the literature. RSM02162 eluted in the same volume as MsAcT in the gel filtration analysis (Experimental Procedures). [d] Identity was determined using Vector NTi (informax/invitrogen) and full-length protein sequences.

the first methionine residues. PROCHECK (*13*) indicates that 94% of the residues are in the core regions with no residues in the disallowed or generously allowed regions of the Ramachandran plot.

Figure Preparation. All graphic figures were prepared with PyMOL (*25*).

Coordinates. Coordinates have been deposited in the Protein Data Bank (accession codes 2q0q and 2q0s).

Determination of the Size of MsAcT in Solution. The solution size of MsAcT was determined by dynamic light scattering using a Malvern Zetasizer, NS.

RESULTS AND DISCUSSION

Enzymatic acylation in water was first observed while investigating the selective oxidation of various alcohols by lyophilized whole cells of *M. parafortuitum*. In the presence of prochiral diols, when ethyl acetate is used as a solvent, a facile transesterification reaction results in the stereospecific acylation of the diols (*6*). The purified protein responsible for this acylation activity is fully active in aqueous reactions containing only millimolar concentrations of ethyl acetate. The sequence of two peptide fragments obtained by cyanogen

bromide cleavage of the enzyme isolated from *M. parafortuitum* eventually led to the identification of the complete gene sequence from the unfinished genome sequence database of *M. smegmatis*, MC_2155. The protein encoded by the identified gene had physical and catalytic properties similar to those of the *M. parafortuitum* protein and was designated MsAcT.

The acyl transfer reaction described above is a replacement of the usual hydrolytic deacylation with an alcoholytic one. A similar reaction involving perhydrolysis would result in the formation of aliphatic peracids and would be an effective source of in situ generated bleaching agents. Lipases that catalyze the formation of peracids for in situ bleaching have been reported previously (*15*), but one of the issues with the commercialization of lipases for this purpose is their inability to efficiently catalyze the reaction in an aqueous environment. MsAcT, however, in the presence of an appropriate substrate (for example, ethyl acetate or ethyl acrylate) and acceptor (for example, neopentyl glycol), preferably catalyzes transesterification at high yield (*6*) (Figure 1). The corresponding hydrolysis reaction was not measured.

To determine whether MsAcT would use hydrogen peroxide as an acceptor, the perhydrolysis:hydrolysis ratio of MsAcT was compared to that of several commercially available lipases. Figure 2 shows the log ratio of perbutyric acid to butyric acid generated by the enzymes in the presence of tributyrin and hydrogen peroxide in an aqueous environment. The specific activity of perhydrolysis by MsAcT was determined to be 700 units/mg of protein at 21 °C with propylene glycol diacetate as the acetate donor and hydrogen peroxide in 100 mM potassium phosphate buffer, pH 7.1. These data demonstrated that in the presence of an acceptor, such as hydrogen peroxide, MsAcT preferably catalyzed the perhydrolysis rather than the hydrolysis reaction, as much as 50-fold over that of the lipases. The ability to produce peracids rapidly in aqueous solution made MsAcT interesting as a potential source for in situ generation of peracids for commercial applications. It was therefore interesting to solve the structure of MsAcT to determine whether there were structural features that contributed to the novel catalysis reactions.

We have determined the structures of MsAcT without and with an inhibitor bound. Crystals of the apoenzyme were obtained in the tetragonal space group *P*4 with eight molecules in the asymmetric unit. The three-dimensional structure of the *M. smegmatis* enzyme was determined to 1.5 Å resolution by MAD techniques using selenomethionine-labeled protein (32 Se in the asymmetric unit). The crystal structure shows that the enzyme is an octamer with eight identical subunits (216 residues per subunit). The octamer can be thought of as a tetramer of closely associated dimers that form a blocklike structure of roughly 72 Å × 72 Å × 60 Å dimensions (Figure 3a) with a large channel in the center running from the "top" to the "bottom" and crevices on the "sides" between pairs of dimers. Each monomer has a five-stranded parallel β-sheet structure sandwiched by α-helices on either side (Figure 3b). The catalytic triad is composed of Ser11, Asp192, and His195. The refined MsAcT octamer model contains 1720 residues (residues 2−216 for all monomers), 8 sulfate ions, 8 glycerol molecules, and 1608 water molecules (Table 2). The crystallographic *R* factor is 17.5%, and R_{free} is 19.6% (using all data without any σ cutoff). The percentages of non-glycine residues in the most favored and allowed Ramachandran areas are 94.2% and 5.8%, respectively, as assessed by PROCHECK (*13*).

Table 2: Summary of Crystal Parameters, Data Collection, and Refinement Statistics for the Apoenzyme

	native enzyme	carbamate-inhibited enzyme
space group	*P*4	*P*1
a (Å)	98.163	67.754
b (Å)	98.163	80.096
c (Å)	229.896	85.974
α (deg)	90.0	104.1
β (deg)	90.0	112.1
γ (deg)	90.0	97.4
monomers/asymmetric unit	8	8
resolution range	30.0−1.5	50.0−1.5
mean $I/\sigma(I)$	14.9 (2.6)[a]	30.8 (8.0)[a]
$R_{sym}(I)$[b]	0.087 (0.208)[a]	0.042 (0.13)[a]
total reflections	327138	302271
completeness	94.7	95.4
R_{cryst}[c]	0.175	0.134
R_{free}[d]	0.196	0.160
protein atoms	13072	13072
sulfate molecule atoms	40	5
glycerol/inhibitor molecule atoms	48	72
solvent molecules	1608	2134
rmsd bond angle	0.015	0.016
rmsd bond angle	1.525	1.627

[a] Highest resolution shell. [b] $R_{sym} = \sum|I_i - \langle I_i\rangle|/\sum|I_i|$, where I_i is the scaled intensity of the *i*th measurement and $\langle I_i\rangle$ is the mean intensity for that reflection. [c] $R_{cryst} = \sum||F_o| - |F_c||/\sum|F_o|$, where F_c and F_o are the calculated and observed structure factor amplitudes, respectively. [d] R_{free} = as for R_{cryst} but for 5.0% of the total reflections chosen at random and omitted from refinement.

A structural homology search performed with MsAcT using the program DALI, which is based on a distance criterion and does not use sequence information for the comparison, revealed five closely related proteins (*16*). These are (1) thioesterase I (PDB code 1ivn) (*17*), (2) platelet-activating factor, an acetylhydrolase (PDB code 1wab), (3) a protein annotated as a hypothetical protein (PDB code 1vjg), (4) esterase (PDB code 1esc), and (5) rhamnogalacturonan acetylesterase (RGAE, PDB code 1deo) (*18*). All of these proteins, along with MsAcT, share a common structural motif (Figure 3b) having a five-stranded parallel β-sheet structure sandwiched by α-helices on either side, characteristic of the SGNH hydrolase fold family (Figure 3c). The active serine resides in a short helical segment following the first β-strand, and the aspartic acid and histidine residues, which form the catalytic triad, are in a loop preceding the C-terminal helix (Figure 3c). In many SGNH hydrolase structures, the helical segment with the active site serine is part of an elbow bend. The various SGNH hydrolases can be differentiated on the basis of the pattern of insertions and deletions from the basic fold that is best exemplified by the *E. coli* thioesterase (*17*).

As found in other SGNH hydrolase structures, the nucleophile Ser11 in the catalytic triad of MsAcT is located in the GDS sequence motif on the short helical segment α1 (Figure 3c), which represents the SGNH block I sequence motif (*19*). The sulfate ion bound at the active site is well defined in the electron density map and makes hydrogen bonds with Ser11 and His195. The sulfate oxygen involved

Table 3: Sequences of Selected SGNH Hydrolases

```
                                                  Insertion 1
M_smegmatisAT          M..AKRILCF GDSLTWGWVP VEDGAPTERF APDVRWTGVL AQQLGADFEV
S_meliloti_RSM2162     MVEKRSVLCF GDSLTWGWIP VKESSPTLRY PYEQRWTGAM AARLGDGYHI
A_radiobacterACA       MV..KSVLCF GDSLTWGSDA ET....GGRH SHDDLWPSVL QKALGPDVKV
E_ColiTAP              ...ADTLLIL GDSLSAGY.. ........RM SASAAWPALL NDKWQSKTSV
A_Aculeatus_1deo       ....TTVYLA GDSTMAK... ......NGGG SGTNGWGEYL ASYL..SATV
                                        Insertion 2
M_smegmatisAT          IEEGLSARTT NIDDPTDPR. LNGASYLPSC LATHLP.LDL VIIMLGTNDT
S_meliloti_RSM2162     IEEGLSARTT SLDDPNDAR. LNGSTYLPMA LASHLP.LDL VIIMLGTNDT
A_radiobacterACA       IHEGLGGRTT AYDDHTADCD RNGARLLPTL LHSHAP.LDL VIIMLGTNDL
E_ColiTAP              VNASISGDTS .......... QQGLARLPAL LKQHQP..RW VLVELGGNDG
A_Aculeatus_1deo       VNDAVAGRS. .......AR. SYTREGRFEN IADVVTAGDY VIVEFGHNDG

M_smegmatisAT          KAYFRR.... .......... .........T PLDIALGMSV LVTQVLTSAG
S_meliloti_RSM2162     KSYFHR.... .......... .........T PYEIANGMGK LVGQVLTCAG
A_radiobacterACA       KPSIHG.... .......... .........S AIVAMKGVER LVKLVRNHVW
E_ColiTAP              LRGFQ..... .......... .......... ....PQQTEQ TLRQILQDV.
A_Aculeatus_1deo       GSLSTDNGRT DCSGTGAEVC YSVYDGVNET ILTFPAYLEN AAKLFTA...
                                                  Insertion 4
                    Insertion 3
M_smegmatisAT          GVGTTYPAPK VLVVSPPPLA PMPHPWFQLI FEGGEQKTTE LARVYSALAS
S_meliloti_RSM2162     GVGTPYPAPK VLVVAPPPLA PMPDPWFEGM FGGGYEKSKE LSGLYKALAD
A_radiobacterACA       QV.PDWEAPD VLIVAPPQLC ETANPVMGAI FRDAIDESAM LAPVYRDLAD
E_ColiTAP              ......KAAN AEPLLMQIRL P......... ANYGRRYNEA FSAIYPKLAK
A_Aculeatus_1deo       ......KGAK VILSSQTPNN PWETGTF... VNSPTR.... FVEYAELAAE

M_smegmatisAT          FMKVPFFDAG .......... ...SVISTDG VDGIHFTEAN NRDLGVALAE
S_meliloti_RSM2162     FMKVEFFAAG .......... ...DCISTDG IDGIHLSAET NIRLGHAIAD
A_radiobacterACA       DLDCGFFDAG .......... ...SVARTTP VDGVHLDAEN TRAIGRGLEP
E_ColiTAP              EFDVPLLPFF ..MEEVY... ...LKPQWMQ DDGIHPNRDA QPFIADWMAK
A_Aculeatus_1deo       VAGVEYVDHW SYVDSIYETL GNATVNSYFP IDHTHTSPAG AEVVAEAFLK

M_smegmatisAT          QVRSLL.... .......... ...
S_meliloti_RSM2162     KVAALF.... .......... ...
A_radiobacterACA       VVRMMLGL.. .......... ...
E_ColiTAP              QLQPLVNHDS .......... ...
A_Aculeatus_1deo       AVVCTGTSLK SVLTTTSFEG TCL
```

in hydrogen bonding with Ser11 also participates in hydrogen bonding with the amide nitrogen of Ala55 and the side chain ND2 of Asn94. Asn94 is the conserved residue present in the block III sequence motif (GXND) of SGNH hydrolase. Unlike the conserved asparagine, Asn94, MsAcT deviates from the SGNH hydrolase by having alanine rather than glycine at position 55, which represents the block II region. Therefore, while we refer to MsAcT as having the SGNH hydrolase fold, it is actually a SANH hydrolase. It is important to note that both alanine and glycine residues function equally well in contributing the amide N to form the oxyanion hole (comprising the N of Ala55, N of Ser11, and ND2 of Asn94). The sulfate ion in the MsAcT structure occupies a similar location as that found for the sulfate ion in RGAE (*18*). Although the overall topology of MsAcT is identical to that of SGNH hydrolases, there are several insertions and one deletion in the MsAcT relative to the general SGNH hydrolase fold (Figure 3d and Table 3) as represented by thioesterase.

Table 1 compares and contrasts what is known about enzymes that share some of the properties of MsAcT and other structurally related enzymes that do not. Of the homologues tested, two proteins, RSM02162 from *S. meliloti* (63.3% identity, 75% similarity) and 7-aminocephalosporanic acid arylesterase (7-ACA) (42.5% identity, 52% similarity) from *A. tumefaciens* (radiobacter) (*20*, *21*), catalyzed perhydrolysis or transesterification, respectively. Indeed, RSM02162 had a significant rate of perhydrolysis, about 50% that of MsAcT (data not shown). From the literature it is known that the *A. tumefaciens* 7-ACA is a tetramer (*20*), while *E. coli* thioesterase and the RGAE are monomers. From gel filtration data, it was determined that MsAcT was an octamer and *S. meliloti* RSM02162, an apparent octamer. It was also demonstrated by dynamic light scattering that the MsAcT octamer was very stable. The protein was diluted in 10-fold dilutions from 21 mg/mL to 21 μg/mL in 100 mM potassium phosphate buffer, pH 7.1. The observed size of 9.3 nm is in good agreement with the dimensions of the octamer reported in this paper determined by X-ray defraction. The observed size of the protein was unchanged by dilution of 4 logs in concentration. The protein was also subjected to incubation in 2 M urea (100 μg/mL) at 50 °C and the size measured for 48 h. No change in the size of the protein or evidence of subunit separation was observed. It appeared that the oligomerization state was a significant structural difference between MsAcT-like enzymes and other SGNH hydrolases and could contribute to the activity.

The oligomeric nature of MsAcT restricts access to and redefines the overall topology of the active site pocket. The structural comparisons show that the monomeric structure of MsAcT superimposes well with the thioesterase structure, with an rmsd of 1.5 Å for 130 Cα atoms (Figure 3d). The

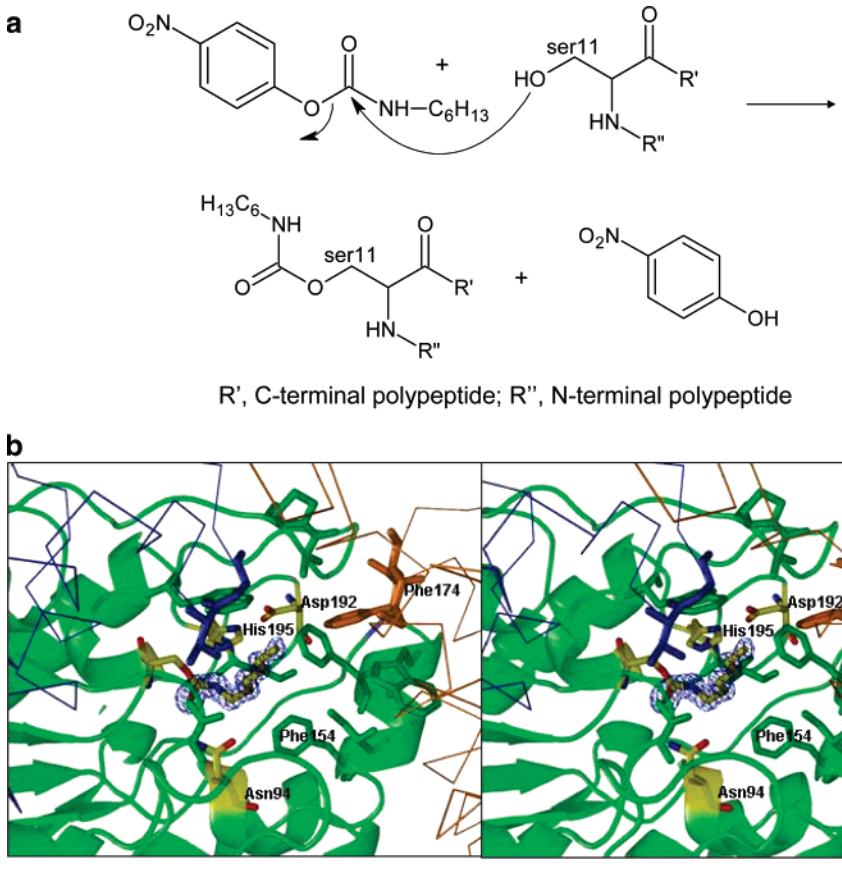

FIGURE 4: Inhibitor bound to the active site. (a) A schematic of the reaction between the 4′-nitrophenyl *n*-hexylcarbamate inhibitor and AcT. (b) Electron density omit map for the inhibitor. The $F_o - F_c$ omit map of the inhibitor is contoured at 4.0σ. The covalently bound inhibitor and the catalytic serine residue are shown in atom colors with carbon atoms in yellow. Important residues are labeled. The side chains of Asp192 and His195, which along with Ser11 form the catalytic triad, are shown as stick models and are color-coded by atom type: green, C; blue, N; red, O. The side chain of Asn94, which along with the amide N atom of Ala55 and Ser11 forms the oxyanion hole, is also shown. Also shown are several side chains that form the hydrophobic channel leading to the catalytic site. Many are found on the same monomer: Trp16, Ala23, Pro24, Ala55 Trp149, Phe150, Ile153, and Phe154 (labeled in the figure). Residues Val125 and Gly126 from the dimer mate monomer, which completes the channel, are shown in blue. The side chain of Phe174 from a third monomer is shown in copper color.

deletion in MsAcT relative to the thioesterase and the other known SGNH hydrolases is between residues 186 and 189. There are four prominent insertions, namely, insertion 1 (residues 17−27), insertion 2 (residues 59−69), insertion 3 (residues 122−130), and insertion 4 (residues 142−156) (Figure 3d and Table 3). These insertions form an elaborated substrate-binding surface and the dimer/octamer interactions (Figure 3e,f). Figure 3e illustrates several key dimer interactions, the most prominent of which is insertion 3, which completes the formation of an elaborated substrate-binding surface formed by insertion loops 1, 2, and 4 of its dimer mate. Figure 3e also illustrates the interaction of several residues, conserved in functionally homologous enzymes, that further stabilizes the dimer. In Figure 3f, the residues in insertion 4 loop interact with neighboring dimer pairs. These interactions contribute to the formation and stabilization of the octamer structure as a tetramer of dimers, with each loop of insertion 4 of a given dimer interacting with different neighboring dimer pairs.

The nature of the substrate-binding pocket was investigated using an inhibitor, 4′-nitrophenyl *n*-hexylcarbamate. The inhibited complex was crystallized in a triclinic space group *P*1 having an octamer in the asymmetric unit (Table 2). Diffraction extended beyond 1.2 Å, and the current model was determined using data collected to 1.25 Å and refined to 1.50 Å resolution. This form contains 1720 residues (residues 2−216 for all monomers), 8 covalently bound inhibitor molecules, 1 sulfate ion, and 2134 water molecules (Table 2). The crystallographic *R* factor and R_{free} are 13.4% and 16.0%, respectively (using all data between 50.0−1.50 Å resolution). The percentages of non-glycine residues in the most favored and allowed Ramachandran areas are 93.8% and 6.2%, respectively, as assessed by PROCHECK.

A schematic of the reaction between the 4′-nitrophenyl *n*-hexylcarbamate inhibitor and AcT is shown in Figure 4a. Electron density was observed for the inhibitor, which is covalently bound to the active site residue Ser11 (Figure 4b). The inhibitor is bound in a hydrophobic channel, which extends to the exterior of the octamer surface, and the position of the alkyl chain indicates the probable direction of substrate approach into the active site. Figure 4b shows that residues forming the hydrophobic channel are derived from three monomers: residues Trp149, Phe150, Ile153, and Phe154 (labeled in Figure 4b) along with Trp16, Ala23, Pro24, and Ala55 (shown in green) from the same monomer, while Val125 (shown in blue) from the dimer mate part of the segment, Gly123, Gly124, Val125, and Gly126, that completes the substrate-binding site (Figure 3e, 4b). The last segment shown in Figure 4b comes from a neighboring dimer that includes Phe174 shown in copper color. While there is

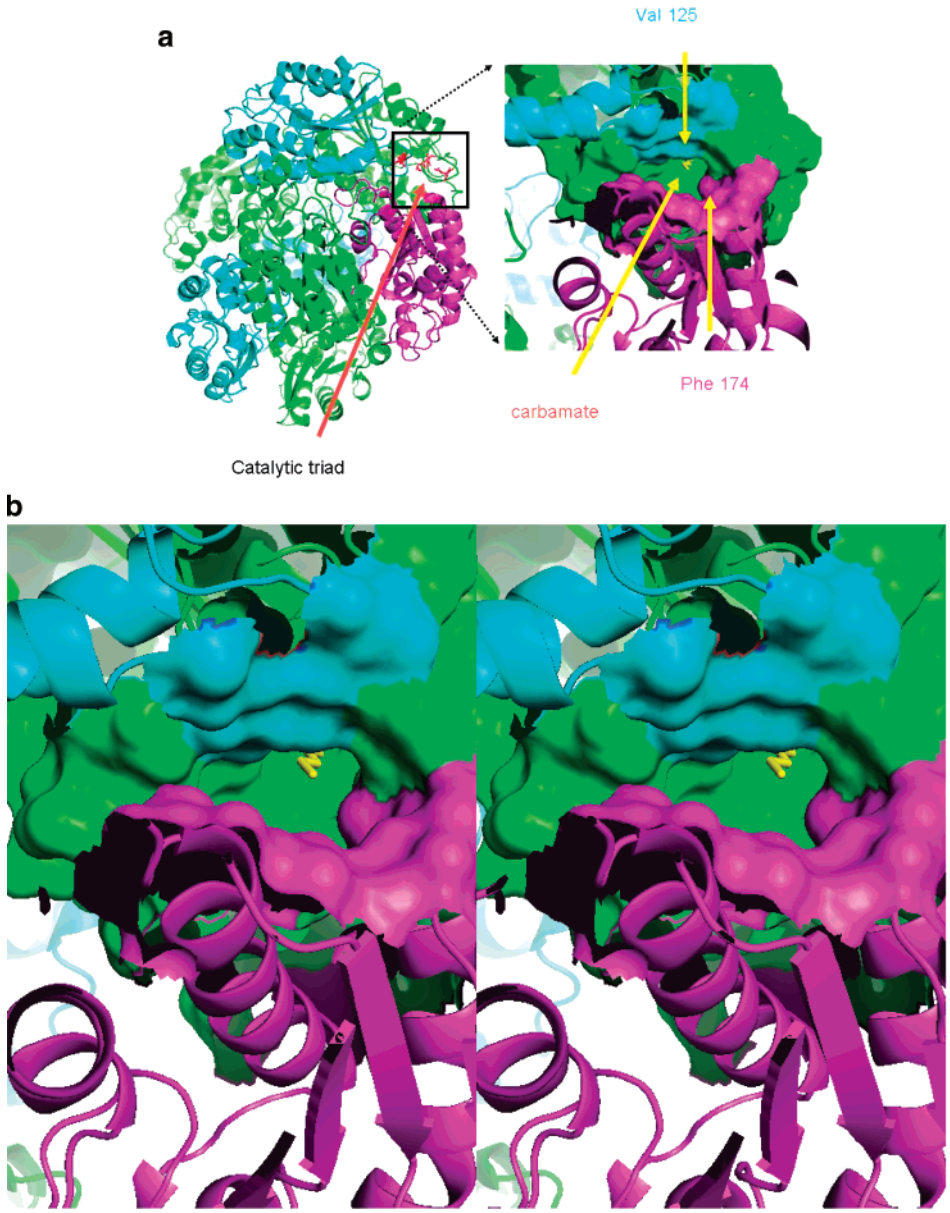

FIGURE 5: Restriction of access to the catalytic site. (a) On the left is an overview of the octamer color-coded similarly to that in Figure 3a. Each of the dimers contains a green- and cyan-colored monomer. The catalytic triad of one green monomer is represented as a stick model and is colored red. The boxed area contains the red catalytic triad and the residues that contribute to the restriction of the active site. The residues are contributed from the catalytic triad parent monomer (green), its dimer mate (cyan), and a third monomer from a neighboring dimer pair (magenta). The boxed area is shown in close-up and in stereo on the right-hand side. Residues from the cyan- and magenta-colored monomers contribute to a channel to restrict access to the reactive center of the green monomer. A yellow stick figure representing the carbamate inhibitor bound to the green monomer is included for reference. One side of the channel is formed by hydrophobic residues from the cyan monomer (A122, A123, G124, V125, G126). The other side of the channel is formed by hydrophobic residues from two segments from the magenta-colored monomer (Leu105, Leu109, Thr116, Val118, Leu119, Phe174, Met175, and Val177). (b) A close-up stereoview of the surface rendering of this restricted hydrophobic channel leading to the catalytic site formed by three monomers shown in (a).

ordered internal water seen in the vicinity, no ordered water is seen in the hydrophobic channel. Moreover, when the enzyme binds the six-carbon inhibitor, it would exclude access to the catalytic center (see Figure 5). The interior of the hydrophobic channel is formed by the four large loops that arise from insertions 1−4 discussed earlier (Figure 3e and Table 3). The restriction of access to the hydrophobic channel arising from the oligomerization is illustrated in Figure 5. Figure 5a shows the region forming the hydrophobic channel leading to the active site of MsAcT in the dimer. The dimer mates are colored green and blue, the exception being the third monomer, which comes from a different dimer pair and also contributes to the restricted access of this channel (colored magenta). The surface relating to the hydrophobic channel is color-coded for the corresponding monomer. Figure 5b shows a stereoscopic close-up of Figure 5a with the yellow stick figure representing the carbamate inhibitor. Furthermore, it is important to note that the access to the active site is controlled by the residues from the "MsAcT-specific" insertion loops (Table 3).

Other than the platelet-activating factor, an acetylhydrolase, which forms a dimer in the crystal structure, all other

SGNH hydrolases with characterized structures are monomeric and do not show any acyltransferase activity in water. The SGNH hydrolases shown in Table 1 were analyzed by sequence alignment (Table 3). It may be seen from the alignments that the SGNH hydrolases that catalyze transesterification/perhydrolysis reactions in water share a common pattern that includes insertions 1−4 as described above. In addition, several specific residues found at dimer and interdimer interfaces are also conserved. Among these are Glu51, Tyr73, and His81 at the dimer interface; Arg101 and Asp106, which form a salt bridge between dimers in the octamer; and Phe174, which along with Leu105 and Leu109 creates a hydrophobic pocket for Trp149 from the insertion 4 loop (Figure 3e,f). All of the enzymes that catalyze acyl transfer in water share the property of appearing in solution as aggregates, either as tetramers or octamers. Moreover, the residues and loops, which form the dimer and interdimer interfaces, are conserved in the sequences of SGNH hydrolases that show acyltransferase activity in water. Therefore, the restricted access to the active site through the hydrophobic channel would be a common feature of these enzymes, and they may form a subclass of enzymes of the hydrolase family. The precise nature and magnitude of the contribution that restricted access provides to favor alcoholysis remain the subject of further experimentation.

The architecture of the MsAcT enzyme provides a structural basis for the control of substrate and the exclusion and partitioning of water that contributes to its ability to catalyze alcoholysis reactions in vast molar excesses of water. In MsAcT this appears to arise from an intricate oligomerization resulting in a highly restrictive reactive channel, which may favor alcoholysis over hydrolysis. This restriction coupled with the hydrophobic nature of the channel would disfavor access to water, normally present in vast molar excess, to allow other moieties such as alcohol and hydrogen peroxide to react with the acyl enzyme intermediate. This finding is similar to the results reported for human β-tryptase where the insertion of loops onto a standard serine protease created an oligomeric enzyme having restricted access linked to its function (*22*). It should now be possible to mimic this natural engineering by modifying other SGNH hydrolases or even lipases from the α/β hydrolases (*23*, *24*) to form new acyltransferases that catalyze transfer reactions in water, creating high value materials for biotechnology and the pharmaceutical industry.

ACKNOWLEDGMENT

We thank the staff at the Advanced Light Source, Berkeley, for their help. Portions of this research were carried out at the Stanford Synchrotron Radiation Laboratory, a national user facility operated by Stanford University on behalf of the U.S. Department of Energy, Office of Basic Energy Sciences. The SSRL Structural Molecular Biology Program is supported by the Department of Energy, Office of Biological and Environmental Research, and by the National Institutes of Health, National Center for Research Resources, Biomedical Technology Program, and the National Institute of General Medical Sciences. We also thank Roopa Ghirnikar for assistance throughout the preparation of the manuscript.

SUPPORTING INFORMATION AVAILABLE

Multiwavelength anomalous data (MAD) collection statistics for the apoenzyme. This material is available free of charge via the Internet at http://pubs.acs.org.

REFERENCES

1. Sym, E. A. (1930) Lipase and its action. The synthetic action of pancreatic lipase in the system: oleic acid-glycerol-water-dissolved lipase, *Biochem J. 24*, 1265−1281.
2. Zaks, A., and Klibanov, A. M. (1985) Enzyme-catalyzed processes in organic solvents, *Proc. Natl. Acad. Sci. U.S.A., 82*, 3192−3196.
3. Klibanov, A. M. (2001) Improving enzymes by using them in organic solvents, *Nature 409*, 241−246.
4. Amin, N. S., Boston, M. G., Bott, R. R., Cervin, M. A., Concar, E. M., Gustwiller, M. E., Jones, B. E., Liebeton, K., Miracle, G., Oh, H., Poulose, A. J., Ramer, S. W., Scheibel, J. J., Weyler, W., and Whited, G. M. (2005) Perhydrolyase, WO2005056782.
5. Hosie, L., Sutton, L. D., and Quinn, D. M. (1987) *p*-Nitrophenyl and cholesteryl-*N*-alkyl carbamates as inhibitors of cholesterol esterase, *J. Biol. Chem. 262*, 260−264.
6. Pettrone, F., Whited, G., and Goodhue, C. (1992) Methods for preparing acetate esters of diols and polyols using *Corynebacterium oxydans* in substantially aqueous media, U.S. Patent No. 5,-114,850.
7. Boston, M., Requadt, C., Danko, S., Jarnagin, A., Ashizawa, E., Wu, S., Poulose, A. J., and Bott, R. (1997) Structure and function engineered *Pseudomonas mendocina* lipase, *Methods Enzymol. 284*, 298−317.
8. Leslie, A. G. W. (1999) Integration of macromolecular diffraction data, *Acta Crystallogr. D55*, 1696−1702.
9. Collaborative Computational Project, Number 4 (1994) The CCP4 suite: programs for protein crystallography, *Acta Crystallogr. D50*, 760−763.
10. Otwinowski, Z., and Minor, W. (1997) Processing of X-ray diffraction data collected in oscillation mode, *Methods Enzymol. 276*, 307−326.
11. Terwilliger, T. C., and Berendzen, J. (1999) Automated structure solution for MIR and MAD, *Acta Crystallogr. D55*, 849−861.
12. Jones, T. A., Zou, J. Y., Cowtan, S. W., and Kjeldgaard, M. (1991) Improved methods for building protein models in electron density maps and the location of errors in these models, *Acta Crystallogr. A47*, 110−119.
13. Laskowski, R., MacArthur, M., Moss, D., and Thornton, J. (1993) PROCHECK: a program to check the stereochemical quality of protein structures, *J. Appl. Crystallogr. 26*, 91−97.
14. Ramachandran, G. N., and Sasisekharan, V. (1968) Conformation of polypeptides and proteins, *Adv. Protein Chem. 23*, 283−437.
15. Wiersma, R. J., Stanislowski, A. G., Gray, G. L., Poulose, A. J., and Power, S. D. (1991) Enzymatic peracid bleaching system, U.S. Patent No. 5,030,240.
16. Holm, L., and Sander, C. D. (1995) A network tool for protein structure comparisons, *Trends Biochem. Sci. 29*, 478−480.
17. Lo, Y. C., Lin, S. C., Shaw, J. F., and Liaw, Y. C. (2003) Crystal structure of *Escherichia coli* thioesterase I/protease I/lysophospholipase L1: Consensus sequence blocks constitute the catalytic center of SGNH hydrolases through a conserved hydrogen bond network, *J. Mol. Biol. 330*, 539−551.
18. Molgaard, A., Kauppinen, S., and Larsen, S. (2000) Rhamnogalacturonan acetylesterase elucidates the structure and function of a new family of hydrolases, *Structure 8*, 373−383.
19. Dalrymple, B. P., Cybinski, D. H., Layton, I., McSweeney, C. S., Xue, G. P., Swadling, Y. J., and Lowry, J. B. (1997) Three Neocallimastix patriciarum esterase associated with the degradation of complex polysaccharides are members of a new family of hydrolases, *Microbiology 143*, 2605−2614.
20. Sakai, Y., Ayukawa, K., Yurimoto, H., Yamamoto, K., and Kato, N. (1998) A novel arylesterase active toward 7-aminocephalosporanic acid from *Agrobacterium radiobacter* IFO 12607: Purification and characterization, *J. Ferment. Bioeng. 85*, 58−62.
21. Sakai, Y., Ayukawa, K., Yurimoto, H., Yamamoto, K, and Kato, N. (1998) A novel arylesterase active toward 7-aminocephalosporanic acid from *Agrobacterium radiobacter* IFO 12607: Nucleotide sequence, gene expression in *Escherichia coli*, and site-directed mutagenesis, *J. Ferment. Bioeng. 85*, 1389−143.

22. Barbosa Pereira, P. J., Bergner, A., Macedo-Ribeiro, S., Huber, R., Matschiner, G., Fritz, H., Sommerhoff, C. P., and Bode, W. (1998) Human β-tryptase is a ring-like tetramer with active sites facing a central pore, *Nature 329*, 306−311.

23. Nardini, M., and Dijkstra, B. W. (1999) α/β hydrolase fold enzymes: the family keeps growing, *Curr. Opin. Struct. Biol. 9*, 732−737.

24. Schrag, J. D., and Cygler, M. (1997) Lipases and α/β hydrolase fold, *Methods Enzymol. 284*, 85−107.

25. DeLano, W. L. (2006) The PyMOL molecular graphics system, DeLano Scientific LLC, Palo Alto, CA (http://www.pymol.sourceforge.net/).

BI7002444